Efficient photorefractive effect triggered by pyroelectricity in magnesium doped $LiNbO_3$ films

ANTON PERIN[1], LUDOVIC GAUTHIER-MANUEL[2], FLORENT BASSIGNOT[3], MATHIEU CHAUVET[2]**

[1]*Tomsk State University of Control Systems and Radioelectronics (TUSUR), 40, prospect Lenina, 634050, Tomsk, Russia*
[2]*FEMTO-ST Institute, UMR CNRS 6174, University of Franche-Comté, 15B avenue des Montboucons, 25000 Besançon, France*
[3]*FEMTO-Engineering, 15B avenue des Montboucons, 25000 Besançon, France*
***Corresponding author: mathieu.chauvet@univ-fcomte.fr*

Received XX Month XXXX; revised XX Month, XXXX; accepted XX Month XXXX; posted XX Month XXXX (Doc. ID XXXXX); published XX Month XXXX

An efficient photorefractive effect triggered by pyroelectricity is demonstrated in slab waveguides constituted of magnesium oxide (MgO) doped $LiNbO_3$ film on insulator. A microwatt-level continuous wave guided at 532nm is self-trapped to form a 10 µm FWHM beam triggered by a only a few degrees temperature increase of the sample. A fast self-focusing response time on the order of milliseconds is measured for milliwatts of injected beam, more than two orders of magnitude faster than in undoped $LiNbO_3$ film. Long lived 2-D induced waveguides are found to be written in the films.

OCIS codes: *(198.4410) Nonlinear optics; (190.5330) Photorefractive optics; (190.5940) Self-action effects; (160.3730) Lithium niobate;*

http://dx.doi.org/10.1364/OL.99.099999

$LiNbO_3$ films (LNF) are at the heart of an intense research activity due to their strong potential for use as RF components [1], exploiting piezoelectric properties, and for the development of integrated optical chips, using electro-optical and nonlinear properties [2-5]. This material is also known as a holographic medium since the discovery of its photorefractive (PR) properties [6] which have been originally applied to induce periodic gratings in bulk crystals [7] and tentatively exploited for integrated optics [8,9]. Later, the discovery of self-trapped beams in SBN crystal, PR spatial solitons [10] has stimulated many related studies. In $LiNbO_3$, dark spatial solitons were first demonstrated thanks to the defocusing photovoltaic effect [11], and later, bright screening solitons with an applied field or relying on the pyroelectric effect have been shown [12-13]. Early on, slab PR waveguides [14] have shown some advantages over bulk media. They provide improved sensitivity and response time and facilitate the implementation of interacting beams due to the initial 1-D light confinement [15,16]. In addition, they open up new configurations such as the control of guided beams using free propagating beams. Finally, the potential applications are enlarged with the possibility of integrating photonic and electronic components in the case of LNF on silicon substrate.

Since the first report in the early eighties of improved $LiNbO_3$ resistance to PR optical damage by doping with magnesium oxide (MgO) [17], this material has become widely used in the photonic industry. In the present study, we show that $LiNbO_3$:Mg films can also exhibit interesting PR properties controlled by a moderate temperature raise. More specifically, fast self-trapping of a 532 nm beam injected in a slab waveguide, constituted of a $LiNbO_3$:Mg film on silica, is reported. The trapped beam induces an optical circuit that is found to be memorized for weeks. We present results studying the full dynamics of the process that reveal the underlying physics. Response time versus intensity is measured and compared with that obtained in undoped congruent $LiNbO_3$ waveguide with a similar structure.

The slab structure is fabricated using a similar process to that in [15]. A 300 nm thick SiO_2 layer followed by sputtering of a 300 nm thick gold layer are deposited by ICPECVD onto one face of a 3-inch diameter 500 µm thick z-cut $LiNbO_3$ sample doped with 5 mol% of MgO. A high flatness 3-inch diameter silicon wafer is also coated with a 300 nm thick gold layer. The metallized faces of both wafers are then brought in contact. This hybrid stacking is then pressed in an EVG wafer bonding machine and high pressure is applied under vacuum at room temperature in order to prevent mechanical stress due to the dissimilar thermal coefficients. At this stage, a 1-mm-thick hybrid structure composed of a $LiNbO_3$ sample bonded to a silicon substrate is obtained. The next step consists in thinning down the sample by grinding and polishing techniques to obtain a 7 µm thick $LiNbO_3$ film with surface roughness of 1-2 nm RMS. To this end, the $LiNbO_3$ layer thickness distribution is assessed by white-light optical reflectometry. The next step consists in using a precision dicing saw equipped with a 56 mm diameter and 400 µm thick equipped with a polishing diamond blade to cut rectangular samples in the hybrid stack.

To optically characterize the waveguides, a 532 nm laser beam is focused to a 10 µm FWHM spot size (Fig. 1a) at the entrance face of the sample. Coupling is adjusted to maximize excitation of the fundamental TM_0 mode of the multimode slab $LiNbO_3$ waveguide. The coupling efficiency is about 12 %. The light distribution at the output of the 2 cm long waveguide is imaged on a camera with microscope objective as depicted in fig. 1a. A mode of 3 µm FWHM height and 143 µm FWHM wide is measured at the output of the waveguide. Note that a slight beam widening (10%) is observed for power above few µW which is attributed to a weak defocusing due the photovoltaic effect.

The sample is placed on a temperature-controlled holder whose temperature is set via a Peltier element. When the temperature is raised above room temperature, the output beam distribution is strongly modified. As an illustration, selected stages of the observed output dynamics are shown in Figs. 1 a-f for an injected power of 60 µW and a temperature increase ΔT=+5 °C. In a first step, the sample temperature is raised 5 °C above room temperature. In a second step, a mechanical shutter is opened to let the incoming beam travel in the waveguide. Self-focusing occurs and forms a minimum beam size of 12 µm FWHM in about one second (Fig. 1c) followed by a transient defocusing (Fig. 1d). Subsequently, a narrow 10 µm FWHM forms again (Fig. 1e). The dynamics ends up with a defocusing process accompanied with the splitting of the beam (Fig. 1f).

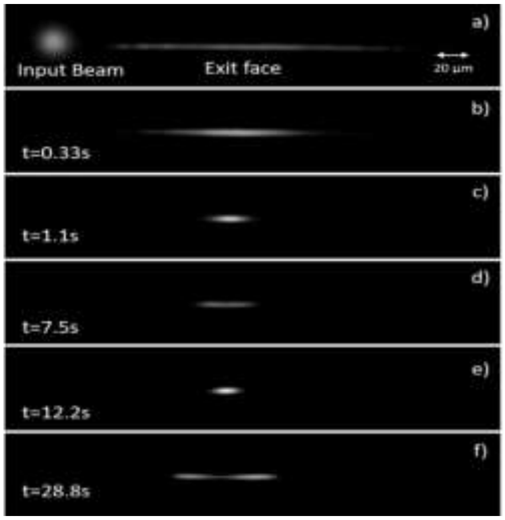

Fig. 1. Images of the input and initial output light distribution in the waveguide (a) and output light evolution for selected times of the self-focusing process when sample temperature is set 5 °C above room temperature (b-f). P_{in}=60 µW.

The dynamics of the beam FWHM evolution is shown in figure 2 for identical parameters as in figure 1 except using a lower power of 7 µW. Note that the origin of the graph time scale is the starting point of the sample temperature increase. The beam is switched on a few seconds after the temperature is stabilized 5 °C above room temperature. Similar features are observed independently of the used light power. The time scale is however reduced as the injected light power is increased. We note that the successive minimum size reached by the beam are not dependent on the intensity with a first minimum close to 12 µm FWHM while the second is narrower with a 10 µm FWHM. To the contrary, the observed transient maximum tends to vanish as intensity is decreased. For instance, 42 µm and 32 µm FWHM are measured at 60 µW and 7 µW, respectively. Following the same procedure, the beam FWHM has been measured at optimum focusing versus ΔT, for a 10µW beam (Fig. 2 inset). As observed for the formation of pyroelectric solitons [13], self-focusing gradually improves as ΔT is increased until beam free diffraction is compensated for ΔT near to 5°C. For larger ΔT values, the output beam FWHM tends to saturate to 10µm enabling an easy implementation of the self-focusing effect. Note that when the temperature is set lower than the room temperature (ΔT<0) an enhanced diffraction is observed (not shown).

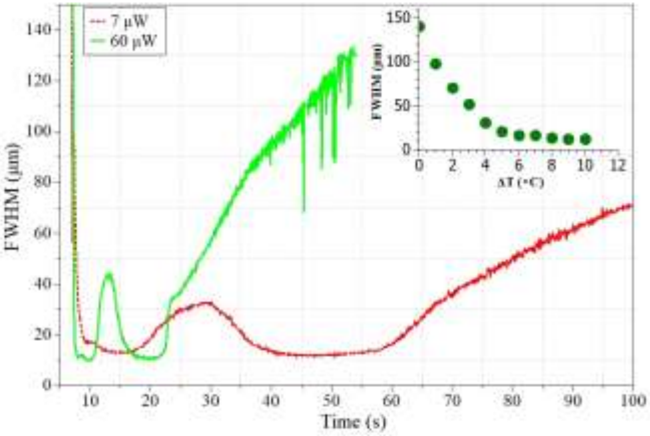

Fig. 2. Measured output beam FWHM as a function of time for two different injected power and optimum focusing FWHM versus ΔT for a 10µW beam (inset).

To characterize the response time, a set of experiments are then performed varying the injected light power when ΔT is set to 5°C. The time to reach the first minimum width is considered in the measurement. The results are shown in figure 3 for the MgO doped waveguide (filled dots) and for a waveguide of similar structure but composed of an undoped 8 µm thick $LiNbO_3$ film (filled triangles). To allow a direct comparison of the response time between the two waveguides, the injected average intensity I at the input is considered. It shows that the MgO doped waveguide exhibits a response time up to two orders of magnitude shorter than in the undoped waveguide. From the slope of the curves we can deduce that the response time decays proportionally to I^{-1} and $I^{-0.5}$ in the MgO and the undoped structures, respectively. For a modest injected intensity of 600 W/cm² (P_{in} ≈ 1 mW) the self-focusing takes place in 50 ms in the MgO waveguide. To overcome the limited frame rate of the camera that does not allow measurements of faster self-focusing response, a programmable shutter is inserted in the optical set-up to control the time of exposure of the writing beam down to millisecond duration. The measurement is performed in two steps. First the writing process is performed for given beam power and exposure time. Then, a weak probe beam is coupled to the induced waveguide to evaluate the size of the guided beam with the camera. With this arrangement, we found that an injected writing intensity of 3000 W/cm^2 (Pin ≈ 5 mW) induces an optimum focused probe beam in 8 ms. From the linear trend of the response (Fig. 3), we can extrapolate that self-focusing would occur in less than a millisecond with an injected beam of thirty milliwatts.

It is important to note that the underlying physics here differs from the one used to model self-focusing in bulk $LiNbO_3$[18]. We emphasize that even though pyroelectric spatial solitons in bulk [13] and films of $LiNbO_3$ both rely on the PR effect, the mechanisms are however modified. Indeed, light induced self-focusing in bulk is due to the well-known classical combined effects of charges photogeneration, transport due to drift by the pyroelectric electric field followed by charges recombination on deep centers in dark area that leads to non-uniform screening of the electric field. It finally induces a refractive index distribution responsible for the self-guiding. In the $LiNbO_3$ film, a simpler mechanism is foreseen. The main reason is that the light guided in the slab waveguide constituted of the $LiNbO_3$ fills the entire thickness of the film. As a consequence, this light bridges the gap between the free charges of opposite sign that are located on the Z+ and Z- faces of the medium due to the pyroelectric effect. The increased conductivity induced by light allows a current to flow between opposite Z-faces giving a rapid electrons-holes recombination. It leads to the decay of the pyroelectric field in the illuminated region and to the nonuniform refractive index distribution at the origin of self-guiding. Self-focusing in z-cut $LiNbO_3$ films is thus a consequence of the neutralization of a charged area through the increased photoconductivity that give rise to the formation of a PR space charge field. This is at the origin of the different observed dynamics in film and in bulk $LiNbO_3$. In addition, this response dominated by the photoconductivity also explains that a faster response is observed in an MgO doped film compare to undoped films (Fig. 3). Indeed, photoconductivity is found to be at least one order of magnitude higher in MgO doped than in undoped $LiNbO_3$ [19].

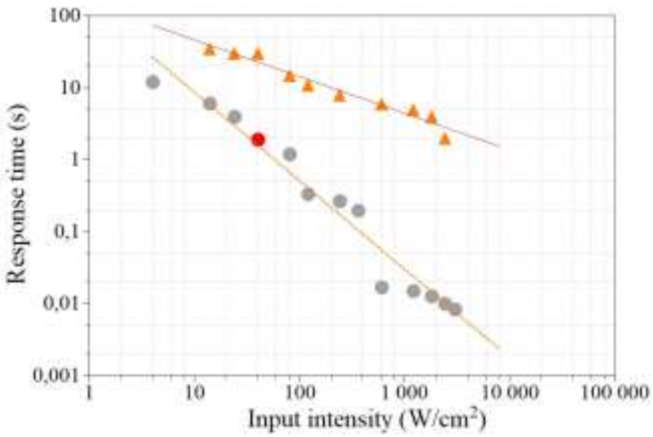

Fig. 3. Response time of the self-focusing effect in $LiNbO_3$ slab waveguides doped with MgO (dots) and undoped (triangles) versus injected intensity and linear fits (dotted lines). The red dot corresponds to the measurement shown in Fig. 1.

To provide further explanations related to the observed transient focusing, we consider the presence of the pyroelectric field along with the impact of the usual defocusing photovoltaic effect for a $LiNbO_3$ layer in open circuit conditions. The dynamics, stemmed from transient spatial solitons [20, 21], is schematically illustrated in figure 4 where the circled charges symbolize fixed charges responsible for the spontaneous polarization of $LiNbO_3$ and non-circled charges are free charges that initially fully compensate the spontaneous polarization. Because of the pyroelectric effect, the amplitude of the spontaneous polarization diminishes [13] when the crystal is heated. This is schematically represented by a lower density of fixed charges in Fig. 4. As a consequence, a net electric field, displayed by the arrows, is present in the direction of the crystal c-axis. In the illuminated area (green spot) the recombination of free charges is facilitated due to the photoconduction that leads to the local electric field decay (Fig. 4a). This induces a lensing effect by the electro-optic effect and a reshaping of the beam propagating inside the crystal until optimum focusing is reached (Fig. 4b). The space charge field continues to evolves with two features (Fig. 4c). Free charges compensation develops on each side of the beam but at a slow pace due to the lower light intensity in this region. While in the central area, where a stronger illumination is present, the pyroelectric field is fully erased and leave place to a field induced by the usual defocusing photovoltaic effect of $LiNbO_3$. These two characteristics explain the simultaneous beam widening and splitting observed for long exposure time. Note that the transient defocusing (Fig. 1c) cannot be explained with this basic model. Some hypothesis such as a competition between deep centers [18] or an oscillatory behavior due to an overfocusing along propagation may be made. To confirm, the development of a specific model for $LiNbO_3$ films would be required which is out of the scope of this paper.

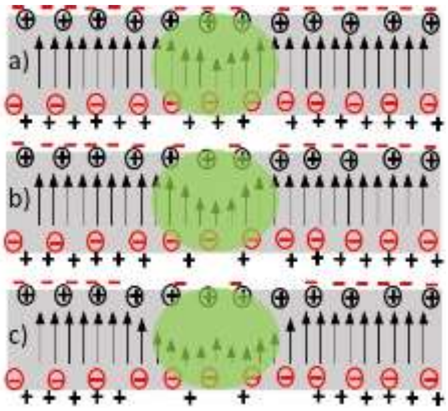

Fig. 4. Schematic description of the charge distribution and space charge field distribution involved in the self-focusing dynamic. Circled charges, non-circled charges, arrows and green spot represents free charges, fixed charges, electric field amplitude and illuminated area, respectively.

The self-focused beam induces a waveguide that can be reconfigured by erasing and further writing. To characterize the properties of this waveguide, an additional set of experiments is performed. One goal is to evaluate the lifetime of the written waveguide. To do so, a self-confined beam is formed with ΔT=5 °C until the optimum confinement is reached as described above. The writing beam is then turned off and the sample temperature is set back to room temperature. A probe beam, at the same wavelength and polarization than the writing beam but strongly attenuated (600nW), is used to monitor the waveguide. This probe is injected in the waveguide to measure the output guided mode horizontal FWHM. The sample is then kept in the dark at room temperature until the next measurement. The evolution of the guided mode normalized FWHM measured over 400 hours is presented by the filled circles in Fig. 5. The guided mode is about seven times narrower than a free propagating probe in the 2cm long sample (filled square). From the slow increase of the guided mode FWHM (slope of dotted line) we can infer that the decay rate is on the order of 5000 hours. This gradual decay can be attributed the thermal contribution to the erasure. Thus, the formed waveguide can be used over a long time when used at a wavelength and/or power for which photoconductivity is negligible. To the contrary, if the structure is exposed to a beam of milliwatt power at a wavelength of 532 nm, the waveguide channel is erased in less than a second. The probe beam fully recovers its free diffraction regime as shown by the filled triangle measurement in Fig. 5. Subsequently, the waveguide can be rewritten to recover the same guiding properties (not shown).

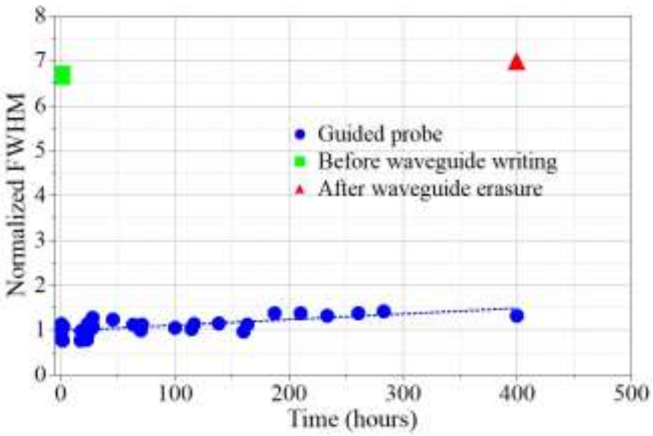

Fig. 5. Measured variation of the normalized output probe beam horizontal size versus time for an induced waveguide kept in the dark (filled circles). Filled square: output probe beam size in the absence of waveguide. Filled triangle: output probe beam size after waveguide erasure.

In conclusion, a fast self-focusing is demonstrated in a slab waveguide consisting of a magnesium oxide (MgO) doped $LiNbO_3$ film on insulator. While the MgO doping is supposed to reduce the PR effect, it is still strong enough to induce an efficient self-trapping when triggered by pyroelectricity. A rich dynamic is observed with response time as short as few milliseconds for few milliwatts beam power beam at 532nm. This short response, which is about two orders of magnitude faster than in undoped $LiNbO_3$ film, is linked to the stronger photoconductivity. The induced index changes are found to form long living 2-D waveguides that can be erased and rewritten. A future development is thus to exploit the green-induced waveguides, triggered by a few degrees temperature increase, to form reconfigurable optical circuits able to propagate light at NIR wavelengths for which PR effect is negligible [22]. The revealed features can also be convenient to induce reconfigurable functions that can be reconfigured rapidly as for optical neural networks [16].

Funding. EIPHI graduate school (ANR-17-EURE-0002); ISITE-BFC project (ANR-15-IDEX-0003); Ministry of Science and Higher Education of the Russian Federation (FEWM-2022-0004).

Acknowledgments. The authors acknowledge the support of the French RENATECH network and its FEMTO-ST technological facility and the Région Bourgogne Franche-Comté. A. Perin acknowledges the financial support of University of Franche-Comté as visiting professor.

Disclosures. The authors declare no conflicts of interest.

Data availability. Data underlying the results presented in this paper may be obtained from the authors upon reasonable request.

References

1. A. Almirall, S. Oliveri, W. Daniau, S. Margueron, T. Baron, P. Boulet, S. Ballandras, S. Chamaly and A. Bartasyte, Appl. Phys. Lett. **114**(16), 162905 (2019).
2. J. Lu, A. Al Sayem, Z. Gong, J. B. Surya, C. L. Zou and H. X. Tang, Optica **8**(4), 539–544 (2021).
3. V. Pecheur, H. Porte, J. Hauden, F. Bassignot, M. Deroh and M. Chauvet, OSA Continuum, **4**(5), 1404–1414 (2021).
4. M. Zhang, C. Wang, P. Kharel, D. Zhu and M Lončar, Optica **8**(5), 652–667 (2021).
5. Y. Zhang, Q. Luo, S. Wang, D. Zheng, S. Liu, H. Liu, F. Bo, Y. Kong and J. Xu, Opt. Lett. **48**(7), 1810–1813 (2023).
6. A. Ashkin, G. D. Boyd, J. M. Dziedzic, R. G. Smith, A. A. Ballman, J. J. Levinsteina and K. Nassau, Appl. Phys. Lett **9**(1), 72–74 (1966).
7. A. Méndez and L. Arizmendi, Opt. Mat **10**(1), 55–59 (1998).
8. R. Müller, M. T. Santos, L. Arizmendi and J. M. Cabrera, J. Phys. D: Appl. Phys **27**(2), 241–246 (1994).
9. Ch. Becker, A. Greiner, Th. Oesselke, A. Pape, W. Sohler and H. Suche, Opt. Lett. **23**(15), 1194–1196 (1998).
10. M. Morin, G. C. Duree, G. J. Salamo and M. Segev, Opt. Lett. **20**(20), 2066–2068 (1995).
11. M. Taya, M. C. Bashaw, M. M. Fejer, M. Segev and G.C. Valley, Phys. Rev. A **52**(4), 3095–3100 (1995).
12. E Fazio, F Renzi, R Rinaldi, M. Bertolotti, M. Chauvet, W. Ramadan, A. Petris and V. I. Vlad, Applied physics letters **85**(12), 2193–2195 (2004).
13. J Safioui, F Devaux and M Chauvet, Opt. Express **17**(24), 22209–22216 (2009).
14. D. Kip, M. Wesner, V. Shandarov and P. Moretti, Opt. Lett. **23**(12), 921 (1998).
15. M. Chauvet, F. Bassignot, F. Henrot, F. Devaux, L. Gauthier-Manuel, H. Maillotte, G. Ulliac and S. Ballandras, Opt. Lett. **40**(7), 1258-1262 (2015).
16. A. Bile, M. Chauvet, H. Tari and E. Fazio, Opt. Lett. **47**(22), 5893–5896 (2022).
17. G. G. Zhong, J. Jian and Z. K. Wu, in Proceedings of the 11th International Quantum Electronics Conference, IEEE Cat. 80, CH 61-0, 631 (1980).
18. F. Devaux, J. Safioui, M. Chauvet and R. Passier, Physical Review A **81**(1), 013825 (2010).
19. J. R. Schwesyg, M. Falk, C. R. Phillips, D.H. Jundt, K. Buse and M.M. Fejer, J. Opt. Soc. Am. B **28**(8), 1973–1987 (2011).
20. N. Fressengeas, D. Wolfersberger, J. Maufoy and G. Kujel, Optics Comm. **145**(1-6), 393–400 (1998).
21. M. Chauvet, J. Opt. Soc. Am. B **20**(12), 2515–2522 (2003).

22. M. Leidinger, C. S. Werner, W. Yoshiki, K. Buse and I. Breunig, Optics Letters, **41**, 5474-5477 (2016).

Full references

1. A. Almirall, S. Oliveri, W. Daniau, S. Margueron, T. Baron, P. Boulet, S. Ballandras, S. Chamaly and A. Bartasyte, “High-frequency surface acoustic wave devices based on epitaxial Z-$LiNbO_3$ layers on sapphire,” Appl. Phys. Lett. **114**(16), 162905 (2019).
2. J. Lu, A. Al Sayem, Z. Gong, J. B. Surya, C. L. Zou and H. X. Tang, “Ultralow-threshold thin-film lithium niobate optical parametric oscillator,” Optica **8**(4), 539–544 (2021).
3. V. Pecheur, H. Porte, J. Hauden, F. Bassignot, M. Deroh and M. Chauvet, “Watt-level SHG in undoped high step-index PPLN ridge waveguides,” OSA Continuum, **4**(5), 1404–1414 (2021).
4. M. Zhang, C. Wang, P. Kharel, D. Zhu and M Lončar, “Integrated lithium niobate electro-optic modulators: when performances meets scalability,” Optica **8**(5), 652–667 (2021).
5. Y. Zhang, Q. Luo, S. Wang, D. Zheng, S. Liu, H. Liu, F. Bo, Y. Kong and J. Xu, “On-chip ytterbium-doped lithium niobate waveguide amplifiers with high net internal gain,” Opt. Lett. **48**(7), 1810–1813 (2023).
6. A. Ashkin, G. D. Boyd, J. M. Dziedzic, R. G. Smith, A. A. Ballman, J. J. Levinsteina and K. Nassau, “Optically-Induced Refractive Index Inhomogeneities in $LiNbO_3$ and $LiTaO_3$,” Appl. Phys. Lett **9**(1), 72–74 (1966).
7. A. Méndez and L. Arizmendi, “Maximum diffraction efficiency of fixed holograms in lithium niobate,” Opt. Mat **10**(1), 55–59 (1998).
8. R. Müller, M. T. Santos, L. Arizmendi and J. M. Cabrera, “A narrow-band interference filter with photorefractive $LiNbO_3$,” J. Phys. D: Appl. Phys **27**(2), 241–246 (1994).
9. Ch. Becker, A. Greiner, Th. Oesselke, A. Pape, W. Sohler and H. Suche, “Integrated optical Ti:Er:$LiNbO_3$ distributed Bragg reflector laser with a fixed photorefractive grating,” Opt. Lett. **23**(15), 1194–1196 (1998).
10. M. Morin, G. C. Duree, G. J. Salamo and M. Segev, “Waveguides formed by quasi-steady-state photorefractive spatial solitons,” Opt. Lett. **20**(20), 2066–2068 (1995).
11. M. Taya, M. C. Bashaw, M. M. Fejer, M. Segev and G.C. Valley, “Observation of dark photovoltaic spatial solitons,” Phys. Rev. A **52**(4), 3095–3100 (1995).
12. E Fazio, F Renzi, R Rinaldi, M. Bertolotti, M. Chauvet, W. Ramadan, A. Petris and V. I. Vlad, “Screening-photovoltaic bright solitons in lithium niobate and associated single-mode waveguides,” Applied physics letters **85**(12), 2193–2195 (2004).
13. J Safioui, F Devaux and M Chauvet, “Pyroliton: pyroelectric spatial soliton,” Opt. Express **17**(24), 22209–22216 (2009).
14. D. Kip, M. Wesner, V. Shandarov and P. Moretti, “Observation of bright spatial photorefractive solitons in a planar strontium barium niobate waveguide,” Opt. Lett. **23**(12), 921 (1998).
15. M. Chauvet, F. Bassignot, F. Henrot, F. Devaux, L. Gauthier-Manuel, H. Maillotte, G. Ulliac and S. Ballandras, “Fast-beam self-trapping in $LiNbO_3$ films by pyroelectric effect,” Opt. Lett. **40**(7), 1258-1262 (2015).
16. A. Bile, M. Chauvet, H. Tari and E. Fazio, “Supervised learning of soliton X-junctions in lithium niobate films on insulator,” Opt. Lett. **47**(22), 5893–5896 (2022).
17. G. G. Zhong, J. Jian and Z. K. Wu, in Proceedings of the 11th International Quantum Electronics Conference, IEEE Cat. 80, CH 61-0, 631 (1980).
18. F. Devaux, J. Safioui, M. Chauvet and R. Passier, “Two-photoactive-center model applied to photorefractive self-focusing in biased $LiNbO_3$,” Physical Review A **81**(1), 013825 (2010).
19. J. R. Schwesyg, M. Falk, C. R. Phillips, D.H. Jundt, K. Buse and M.M. Fejer, “Pyroelectrically induced photorefractive damage in magnesium-doped lithium niobate crystals,” J. Opt. Soc. Am. B **28**(8), 1973–1987 (2011).
20. N. Fressengeas, D. Wolfersberger, J. Maufoy and G. Kujel, “Build up mechanisms of (1+1)-dimensional photorefractive bright spatial quasi-steady-state and screening solitons,” Optics Comm. **145**(1-6), 393–400 (1998).
21. M. Chauvet, “Temporal analysis of open-circuit dark photovoltaic spatial solitons,” J. Opt. Soc. Am. B **20**(12), 2515–2522 (2003).
22. M. Leidinger, C. S. Werner, W. Yoshiki, K. Buse and I. Breunig, “Impact of the photorefractive and pyroelectric-electro-optic effect in lithium niobate on whispering-gallery modes”, Optics Letters, **41**, 5474-5477 (2016).